Transient wave-leak interaction analysis for improved leak detection in viscoelastic pipelines

Ying Zhang [a]; **Huan-Feng Duan** [a, *]; **Alireza Keramat** [a, *]; **Bin Pan** [a, *]; **Silvia Meniconi** [b];

Bruno Brunone [b]; **Pedro J. Lee** [c]

[a] Department of Civil and Environmental Engineering, The Hong Kong Polytechnic University,

Hung Hom, Kowloon, Hong Kong SAR, 999077, PR China

[b] Department of Civil and Environmental Engineering, The University of Perugia,

Via G. Duranti 93, Perugia 06125, Italy

[c] Department of Civil and Natural Resources Engineering, The University of

Canterbury, Private Bag 4800, Christchurch, New Zealand

*Corresponding authors, E-mail: *hf.duan@polyu.edu.hk; alireza.keramat@polyu.edu.hk;*

bin.pan@connect.polyu.hk.

Abstract

Transient wave reflection methods (TWRMs) have exhibited favorable capability in leak detection for elastic pipelines, but applications have also demonstrated their relatively low accuracy for viscoelastic pipelines. This paper investigates the transient wave behaviour, the principal tenet for leak detection by TWRMs, in a leaky viscoelastic pipeline to understand the mechanism of wave modification by leaks and viscoelasticity. Based on the correspondence principle, this research derives analytical formulations of the leak-induced wave reflection and phase difference at any measurement point in a viscoelastic pipe. According to the measured reflection coefficient, an optimization algorithm is further developed to estimate the leak location and size. The methodologies are then assessed and discussed for sinusoidal and sigmoid perturbations through numerical and laboratory tests. The extensive analyses indicate that: (i) Taking steady friction and unsteady friction into account in deriving the reflection coefficient of a leaky viscoelastic pipe contributes to improving the accuracy of leak detection; (ii) the damping effect caused by the viscoelasticity of the pipe wall material is more significant with the measurement distance while the viscoelasticity-induced wave phase shift decreases with the measurement distance; (iii) leak ratio affect the magnitude of the reflected wave, but the wave phase shift is relatively independent of the leak ratio for practical applications.

1. Introduction

Viscoelastic pipelines that are made of plastic or polymeric materials, such as polyvinyl chloride (PVC), polyethylene (PE), high-density polyethylene (HDPE), and polypropylene-random (PPR), are increasingly applied in water conveying pipelines due to their advantages of competitive low price, high flexibility, low overall failure rate (anti-corrosion, anti-vibration, surge protection) and convenience in transportation and installation [1-5]. In urban water supply systems, fast flow variations can be commonly caused by the adjusting control facilities and/or by a change in boundary conditions [6-9], which in turn induce a sharp pressure change propagating in the pipe, that is referred to as hydraulic transients (i.e., transient waves). Hence, understanding the propagation behaviour of such transient pressure waves in viscoelastic pipes and their interaction with the pipeline's physical discontinuities or boundaries forms the tenet of existing transient wave reflection-based methods (TWRMs) for anomaly detection in pipes [10-12] such as leaks. This in turn provides insights for effective water loss management and intelligent network establishment.

Unlike elastic pipes (metal or concrete pipes) whose mechanical properties are somehow time-independent, viscoelastic material's response to transient loads presents high complexity [13] due to their long molecular chain structures, which thus depends on the temperature, stress-time history, and pipe axial and circumferential constraints, etc. Under transient flow conditions, a generalized Kelvin-Voigt model with one or multiple elements containing a spring and a dashpot in parallel (representing the retarded strain), connected in series to a single spring (representing the instantaneous strain) is proved as an additional term in the continuity equation of the transient flow (water hammer) to capture the retarded response of viscoelastic pipes. Although laboratory mechanical tests such as creep tests on pipe materials can give a preliminary estimation of the viscoelastic parameters of the Kelvin-Voigt model, these values are usually obtained under

3

relatively static/stationary conditions, which cannot accurately represent the pipe-wall viscoelasticity under operation states, especially for transient flow conditions [1, 2, 5]. Consequently, many calibration approaches have been explored in recent references to obtain more reliable viscoelastic parameters (VEP) in polymeric pipeline systems through hydraulic transient tests [1, 2, 5, 14, 15]. For example, Wang, et al. [2] developed a VEP estimation method that does not need any information about leaks and instead applies the principle that a practical leak size does not shift the phase of the wave. More specifically, their study assumes that the steady-state cross-time of the transient pressure signal keeps invariant to a leak and the wave phase shift is only due to the viscoelasticity. In the frequency domain, Pan, et al. [1] proposed an efficient inverse transient analysis procedure to calibrate VEP simultaneously and detect leaks (location and size) in both single and branched pipes based on the leak-induced pattern, which presents an improvement compared to the multi-stage VEP calibration method developed in the previous study [14]. Meanwhile, Gong, et al. [15] proposed a fast and efficient process that only uses information about the resonant frequencies of the pipeline. This method can calibrate not only the VEP but also the elastic component of the wave speed. In fact, all these developed transient-based calibration procedures for VEP have put forward the foundation for accurate faults detection in viscoelastic pipelines.

Regarding transient modeling of viscoelastic pipes, the one-dimensional model [2, 5, 16-19], or the quasi-two-dimensional model [4, 13], coupled with different dynamic factors such as fluid-structure interaction [3, 20, 21], unsteady friction [4], air-fluid interaction effects [22], in combination with discontinuity equation (joins, blockages, leaks) [11, 18, 21, 23-25] have been developed to simulate the transient wave behaviour along the pipeline. Besides, due to the unavoidable noise impacts and other uncertainties on the measured transient signals in real-life

4

water pipelines, a newly developed signal processing technique by Wang, et al. [26], named as matched field processing method, has been successfully applied to the experimental laboratory tests containing an HDPE pipe for leak location detection. The numerical and laboratory results of the former studies, e.g., [27-29], indicate that viscoelasticity induces both dampings to the transient pressure peaks and smoothing to the physical signatures on the collected signals, which is also manifested in the wave speed. The wave speed is a frequency-dependent complex-valued function in viscoelastic pipes, as revealed in the transfer matrix or standard impedance method used to simulate the transient pipe flows [15, 30, 31]. In the time domain, it decreases with the wave periods rather than being constant as it is in the elastic pipes [2, 5, 31].

As for transient behaviour in a viscoelastic pipeline with leaks, current studies mainly focus on the frequency domain. They are mostly, based on the analytical solutions that leaks modify the amplitude of the system frequency response function (also termed as leak-induced patterns), which then can be inversely applied to detect leaks (location and size) and viscoelastic parameters by measuring the transient response in both a single pipeline [1, 18, 25] and complex pipe systems [1, 32]. Despite various works on the above-mentioned leak-induced pattern analysis, very limited information about the leak-induced reflection coefficient in the frequency domain in a viscoelastic pipe is reported. Although several research works, e.g., [1, 25, 26], are dedicated to the theoretical evidence of the leak reflection and viscoelasticity in the frequency domain, the leak reflection and phase shift following a single-frequency wave in the time domain are not yet elaborated. One of the possible reasons may be attributed to the more severe attenuation and retardation of the transient pressure waves in a viscoelastic pipeline in the time domain, making leak location and sizing more difficult than the elastic pipes or the frequency domain techniques.

TWRM is a time-domain approach, in which the leak location is estimated by the arrival time

of the leak-induced reflection signals with the preliminary known wave speed [10], while the leak size is approximated by measuring the ratio of the magnitude of reflection waves to that of the corresponding incident one at measurement points [10, 33, 34]. Many previous applications of this TWAM for the leak size estimation in viscoelastic pipes are based on the following simplified hypotheses: (i) frictionless pipeline [35]; (ii) elastic pipe-wall though testing viscoelastic pipes [10, 29, 34]. Consequently, the amplitude damping and phase shift effects of transient waves in viscoelastic pipes cannot be properly accounted for by the current TWRM. The main reason for neglecting these two effects is the difficulty in analytically treating the friction-related nonlinear term and viscoelastic-related retard strain term in the complex transient models. Although acceptable results were reported for some specific case studies in the literature, still the inclusion of these two effects in the derivation of the reflection coefficient helps enhance the accuracy and applicability of this type of TWRM for practical applications. Furthermore, a recent study by Zhang, et al. [36] has indicated the significant impact of measurement distance on the application of TWRM for leak detection in an elastic pipe, which may also form an issue for viscoelastic pipelines. To this end, it is necessary to perform a systematic analysis for the leak-induced reflection wave and its propagation considering both friction and viscoelasticity effects as well as the measurement distance influence, which is the motivation and scope of this study.

2. Methodology

This section presents the main methods and key results for the transient wave behaviour in a leaky viscoelastic pipeline based on theoretical and analytical derivations.

2.1.1 Leak-induced reflection coefficient

The classic one-dimensional (1D) transient flow model (water hammer model) for elastic pipes in the time domain can be expressed by the continuity and momentum equations as follows [37]:

$$\frac{\partial \tilde{Q}}{\partial x} + gA\left(\frac{\rho}{K} + 2\frac{C}{g}J_0\right)\frac{\partial \tilde{H}}{\partial t} = 0 \tag{1}$$

$$\frac{1}{gA}\frac{\partial \tilde{Q}}{\partial t} + \frac{\partial \tilde{H}}{\partial x} + \text{sign}(Q)\frac{f_D}{2gDA^2}\left(2Q_0\tilde{Q} + \tilde{Q}^2\right) + C_J\int_0^t W(t-t')\frac{\partial \tilde{Q}}{\partial t'}dt' = 0 \tag{2}$$

in which $\tilde{H}$ = pressure head deviation (or perturbation) from the mean; $\tilde{Q}$ = discharge deviation (or perturbation) from the mean; D = pipe diameter; A = cross-sectional area of pipe; f_D = Darcy-Weisbach friction factor; ρ = density of fluid; g = gravitational acceleration; K = bulk modulus of fluid; $J_0 = 1/E_0$; E_0 = bulk modulus of elasticity; $C = \rho g \varphi D/(2e)$; φ = pipe constraint coefficient; e =pipe-wall thickness; $C_J = 16v/(gD^2A)$; v = kinematic viscosity (m²/s); $W(t) = \phi_w e^{-\lambda t}/\sqrt{\pi t}$ = weighting function of the unsteady friction model for turbulent flows [38];

$\phi_w = D/(4\sqrt{v})$; $\lambda = 0.54vk_R/D^2$; $k_R = \text{Re}_0^{\log(14.3/\text{Re}_0^{0.05})}$; t = temporal coordinate; x = spatial coordinate along the pipeline. This simplified governing equation set derived from the Reynolds Transport Theorem [6] is based on the following major assumptions: (1) the fluid is slightly compressible; (2) the pipe wall is slightly deformable; (3) the convective acceleration terms are neglected; (4) the pipe slope is so small that can be neglected.

Under transient pipe flow conditions, the acoustic wave speed in a fluid pipeline can be defined as,

$$a_0 = \left(\frac{\rho}{K} + 2\frac{C}{g}J_0\right)^{-\frac{1}{2}} \tag{3}$$

where a_0 = elastic (or pre-transient) component of acoustic wave speed. To obtain the analytical solution of these equations, a Laplace transform [39] is taken from Eqs. (1) and (2) accompanied

by several mathematical manipulations (for more details please refer to Appendix A), yielding:

$$\hat{\tilde{Q}}_{xx}(x,s) + \mu_E^2 \hat{\tilde{Q}}(x,s) = 0 \tag{4}$$

in which $\hat{\tilde{Q}}(x,s)$ is the Laplace transform of $\tilde{Q}(x,t)$, the subscript xx represents the second partial

derivative of the variable with respect to x, $s = jw =$ Laplace variable, and

$$\mu_E^2 = -\left(\frac{s^2}{a_0^2} + \frac{s^2 gAC_J \phi_w}{a_0^2} \sqrt{\frac{1}{s+\lambda}} + sign(Q) \frac{sgAR}{a_0^2} \right) \tag{5}$$

where μ_E is propagating operator, subscript E represents elastic quantity and $R = \frac{f_D Q_0}{gDA^2}$ is steady-

state resistance term for turbulent flows.

The incorporated transient model in the following sections disregards the structural vibration

impacts on the transient pressures [21, 40, 41]. However, as discussed in [21], the impact of the

soil surrounding the buried pipes causes the pipe wall to develop a delay between the applied load

(pressure) and responses (pipe deformation). This creep behavior can partially be modeled by a

constitutive viscoelastic model for the pipe wall, which is not the focus of this research. Therefore,

according to the correspondence principle, the Laplace transform of the viscoelastic solution (as

shown in Eqs. (4) and (5)) can be directly obtained from the existing elastic solution [42] by

replacing J_0 in Eq. (3) with the creep function of the viscoelastic material in the Laplace domain

$\hat{J}^* = s\hat{J}(s)$ and by replacing a_0 in Eq. (3) by a_{VE} [20], there are:

$$a_{VE} = \left(\frac{\rho}{K} + 2\frac{C}{g}\hat{J}^* \right)^{-\frac{1}{2}} \tag{6}$$

which is consistent with the viscoelastic wave speed derived in the references [3, 26], with

subscript VE for viscoelastic quantity. As a result, Eq. (5) becomes,

$$\mu_{VE}^2 = -\left(\frac{s^2}{a_{VE}^2} + \frac{s^2 gAC_J \phi_w}{a_{VE}^2} \sqrt{\frac{1}{s+\lambda}} + sign(Q) \frac{sgAR}{a_{VE}^2} \right) \tag{7}$$

in which μ_{VE} is a complex number and can be further decomposed into $\mu_{VE} = \mu_{VE,r} + j\mu_{VE,j}$. The real part $\mu_{VE,r}$ and the imaginary part $\mu_{VE,j}$ govern the transient wave phase shift and damping behaviour, respectively [36]. In Eq. (6), the creep function in the time domain is represented by:

$$J(t) = J_0 + \sum_{i=1}^{N_{KV}} J_i\left(1 - e^{-t/\tau_i}\right) \tag{8}$$

where $J_0 = 1/E_0$ provides instantaneous (or elastic) response of the pipe wall's strain; $J_i = 1/E_i$ = creep compliance of the spring of the i-th Kelvin-Voigt element, representing deformability of the viscoelastic pipe [14]; $\tau_i = \vartheta_i/E_i$ = retardation time of the i-th Kelvin-Voigt element, that describes the frequency shift of transient waves [1, 43]; subscript i is the element number in the generalized Kelvin-Voigt model (see Fig. 1); e = Napier number; N_{KV} = total number of the elements; E_0, E_i = modulus of elasticity of the single spring and the spring of the i-th Kelvin-Voigt element, respectively; and ϑ_i = dynamic viscosity corresponding to the i-th dashpot.
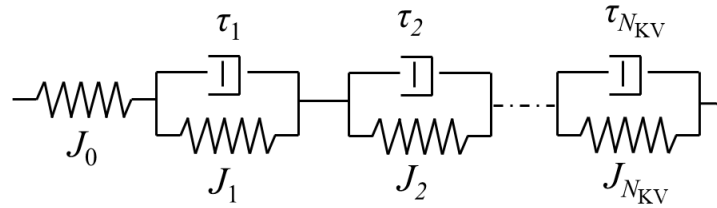
Figure 1 Generalized Kelvin-Voigt model

Applying the Laplace transform to Eq. (8) leads to

$$\hat{J}^* = s\hat{J}(s) = s\left(\frac{J_0 + \sum_{i=1}^{N_{KV}} J_i}{s} - \sum_{i=1}^{N_{KV}} J_i \frac{1}{s - \left(-\frac{1}{\tau_i}\right)}\right) \tag{9}$$

As a result, an ordinary differential equation for a viscoelastic pipeline can be obtained:

$$\hat{\bar{Q}}_{xx}(x,s) + \mu_{VE}^2 \hat{\bar{Q}}(x,s) = 0 \tag{10}$$

9

The solution to Eq. (10) is

$$\hat{\bar{Q}}(x,s) = \hat{\bar{Q}}^{ref} e^{\frac{s\mu_{VE}}{w}x} + \hat{\bar{Q}}^{tr} e^{-\frac{s\mu_{VE}}{w}x} \tag{11}$$

where $\hat{\bar{Q}}^{tr}$ and $\hat{\bar{Q}}^{ref}$ are the flow amplitude of the wave traveling in the positive (i.e., transmitted part) and in the negative direction (i.e., reflected part)[44], respectively. Taking the partial derivative of Eq. (11) with respect to x and substituting the result into the Eq. (10) yields (Appendix (A.1))

$$\hat{\bar{H}}(x,s) = -\hat{\bar{H}}^{ref} e^{\frac{s\mu_{VE}}{w}x} + \hat{\bar{H}}^{tr} e^{-\frac{s\mu_{VE}}{w}x} \tag{12}$$

in which

$$\hat{\bar{H}}^{ref} = k_{VE}\hat{\bar{Q}}^{ref}, \ \hat{\bar{H}}^{tr} = k_{VE}\hat{\bar{Q}}^{tr}, \ k_{VE} = \frac{\mu_{VE} a_{VE}^2}{gAw} \tag{13}$$

Assuming that the head and flow perturbation are sinusoidal oscillations and can be represented in exponential forms [45, 46] as follows:

$$\tilde{H}(x,t) = Real(\hat{\bar{H}}e^{st}) = Real\left\{\left(-\hat{\bar{H}}^{ref} e^{\frac{s\mu_{VE}}{w}x} + \hat{\bar{H}}^{tr} e^{-\frac{s\mu_{VE}}{w}x}\right)e^{st}\right\} = Real(f + F) \tag{14}$$

$$\tilde{Q}(x,t) = Real(\hat{\bar{Q}}e^{st}) = Real\left\{\left(\hat{\bar{Q}}^{ref} e^{\frac{s\mu_{VE}}{w}x} + \hat{\bar{Q}}^{tr} e^{-\frac{s\mu_{VE}}{w}x}\right)e^{st}\right\} = Real\left\{\frac{1}{k_{VE}}(-f + F)\right\} \tag{15}$$

where $f = -\hat{\bar{H}}^{ref} e^{s\left(\frac{\mu_{VE}}{w}x+t\right)}$ = reflected wave function, $F = \hat{\bar{H}}^{tr} e^{s\left(-\frac{\mu_{VE}}{w}x+t\right)}$ = incident wave function. These two equations indicate that the perturbation of pressure head and flow rate at arbitrary space and time point (x, t) can be evaluated by these two traveling wave functions. The combination of Eqs. (14) and (15) can be used to solve the magnitude of the transmitted and reflected wave when a transient pressure wave arrives at a leak.

As illustrated in Fig. 2, the pressure and flow rate change at the leak after the transmission of the approaching transient pressure wave F_1.
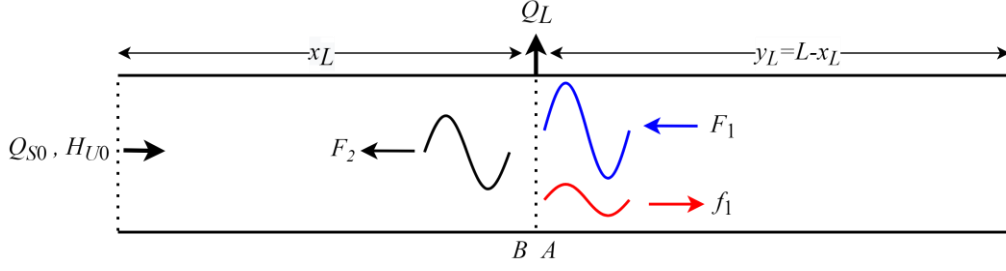
Figure 2 Sketch of the transient incident wave and reflected waves from a leak

Let points *A* and *B* in Fig. 2 represent the virtual vicinal downstream and upstream of the leaky point. The transmission of F_1 is represented by F_2 and its reflection is represented by f_1. The reflected wave f_1 at the leaky point has the following form (for details, refer to Appendix B):

$$f_1 = \frac{1}{8}\frac{(k_{VE}\alpha Q_{S0})^2}{H_{L0}} + \frac{k_{VE}}{2}\alpha|Q_{S0}| - \frac{1}{2}\frac{k_{VE}}{2}\frac{\alpha|Q_{S0}|}{\sqrt{H_{L0}}}\sqrt{\left(\frac{k_{VE}}{2}\frac{\alpha Q_{S0}}{\sqrt{H_{L0}}}\right)^2 + 4\left(\frac{k_{VE}}{2}\alpha|Q_{S0}| + H_{L0} + F_1\right)} \quad (16)$$

where $\alpha = Q_{L0}/Q_{S0}$ =leak ratio, Q_{S0} is the steady-state flow rate at the upstream point of the leak. From this equation, it is clear that f_1 theoretically relates to the leak characteristics (leak ratio α and the steady-state local pressure at the leak H_{L0}), initial condition Q_{S0}, incident transient pressure wave F_1 and wavenumber k_{VE}. To quantify the leak-induced reflection coefficient at the leak C_{ref_L} is defined as the ratio between the amplitude of the reflected wave and the incident wave:

$$C_{ref\_L} = \frac{|f_1|}{|F_1|} \quad (17)$$

The derivation of this variable and its application is elaborated in the following.

2.1.2 Reflection coefficient at the measurement point

For a physically continuous pipe section, the propagation of a Fourier mode (sine wave) can be represented as [47]:

$$\tilde{H}(x,t) = Real(\widehat{\tilde{H}}^{tr}e^{-\frac{s\mu_{VE}}{w}x}e^{st}) = Real\left\{\widehat{\tilde{H}}^{tr}e^{\mu_{VE,j}x}e^{s\left(t-\frac{\mu_{VE,r}}{w}x\right)}\right\} \qquad (18)$$

Hence, the pressure oscillation amplitude with space can be obtained as,

$$h_{amp} = \left|\widehat{\tilde{H}}^{tr}\right|e^{\mu_{VE,j}x} \qquad (19)$$

where x is the distance that the pressure wave has traveled, $\mu_{VE,j}$ describes the frequency-dependent attenuation by the viscoelasticity and friction effects along a pipeline, and the absolute value symbol represents the magnitude of a complex number. This equation shows that the pressure wave amplitude dampens exponentially with the distance it travels.

Considering the attenuation and reflection during the overall wave travel, the desired ratio of reflected amplitude to the incident wave at the measurement point is (for detailed derivation, refer to Appendix C):

$$C_{ref\_M} = C_{ref\_L}e^{\mu_{VE,j}(2d)} \qquad (20)$$

The analytical solution in Eq. (20) indicates that the reflection coefficient at the measurement point depends not only on the reflection coefficient at the leak but also on the distance between the leak and measurement location d, friction effects (steady friction and unsteady friction), pipe-wall viscoelasticity, and wave frequency w. Based on this solution, it also gives a hint that leak location d and leak ratio α can be calculated by optimization algorithms that match this theoretical reflection coefficient to the measured values. Note that, for the case of an elastic pipe, the reflection coefficient whose damping is only due to the friction effects [48, 49], can be obtained by replacing μ_{VE} (in Eq. (7)) by μ_E (in Eq. (5)), which eventually leads to the same result in [36].

2.1.3 Transient wave phase difference along the pipeline

In practical problems, little attention has been paid to the phase response of transient waves

compared with the amplitude response. This is because of the real practice difficulty in measuring the phase difference directly [50], such as the asynchronous timing of the gated counter with the signals and ultra-high frequency requirement for the counter [51].

According to the wave function presented by Eq. (18), it not only indicates the damping information (attenuation) of the traveling transient pressure wave oscillation but also gives the phase information (dispersion). To make it clearer, we rewrite this equation as follows:

$$\tilde{H}(x,t) = Real(\hat{\tilde{H}}^{tr}e^{\mu_{VE,j}x}e^{s\left(t-\frac{\mu_{VE,r}}{w}x\right)}) \overset{s=jw}{\Longrightarrow} Real(\underbrace{\hat{\tilde{H}}^{tr}e^{\mu_{VE,j}x}}_{amplitude\ damping}\ e^{\overset{j(wt-\mu_{VE,r}x)}{phase}}) \quad (21)$$

Hence, the phase difference θ of the incident wave at the two measurement points can be represented by:

$$\theta = \Delta(wt - \mu_{VE,r}x) = w\Delta t - \mu_{VE,r}\Delta x \quad (22)$$

where w is the angular frequency of the input signal; Δt and Δx are the pressure wave's traveling time and traveling distance from one location to another location, respectively. For a viscoelastic pipe, the pressure wave's phase difference during propagation is dependent on the pipe-wall viscoelastic parameters, friction-dependent loss, and wave frequency that are characterized by $\mu_{VE,r}$. Furthermore, θ can be normalized by 2π:

$$\theta^* = \theta/(2\pi) \quad (23)$$

Numerically (i.e., pressure wave generated by the model) or experimentally, the phase difference of the incident wave at two measurement points in the time domain (as visualized in Fig. 3) is calculated by the time-delay of the characteristic points of the signals (peaks, troughs, zero-crossing values) [52] or obtained using the cross-correlation technique [53]. Here, we choose the former method to characterize dimensionless phase difference θ^* as follows:

$$\theta^* = \frac{(t_2^P - t_1^P)}{T_{in}} \quad (24)$$

in which, t_1^P and t_2^P are the occurrence time of the same pressure characteristic points (here, we choose pressure peak, notated as superscript P) at the two measurement points with respect to their oscillation starting points, respectively; T_{in} is the wave period. $\theta^* = 0$ means that there's no phase difference and $\theta^* > 0$ means that the time delay (or time shift) occurs during pressure wave propagation. For viscoelastic materials, the phase difference between the applied sinusoidal strain and the corresponding stress (or vice versa) is obtained based on the ratio of the loss modulus to storage modulus in dynamic mechanical testing, which has a value range of $0 \sim 90°$ (or $0 \sim \pi/2$).
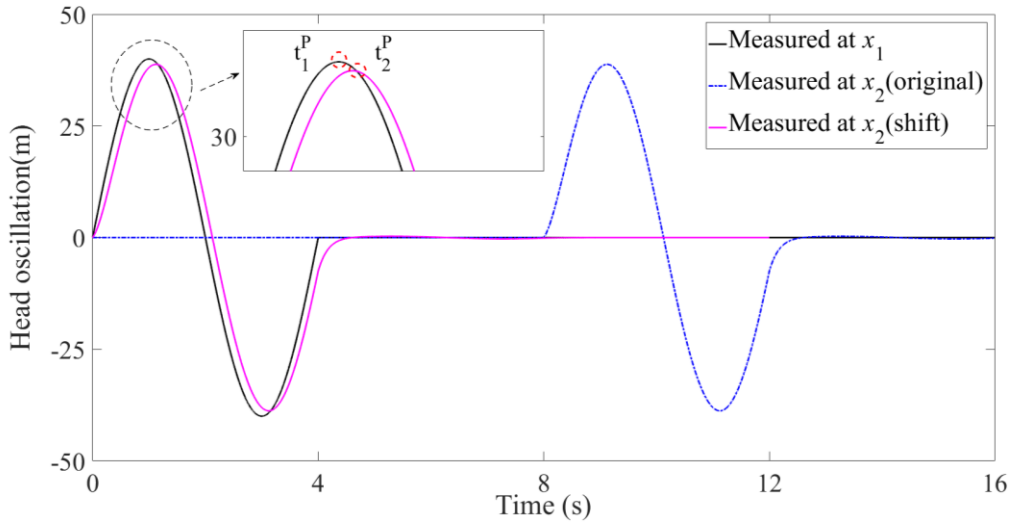

Figure 3 Illustration of the phase difference of pressure traces by two sensors

2.2 Leak detection procedure

Based on the derived reflection coefficient above, the overall leak detection procedure of the TWRM can be summarized in Fig. 4. In detail, for numerical or experimental applications, a transient signal is firstly injected into an unbounded hypothetical leaking system (with pipe length L, quasi-steady friction factor f_D and initial upstream flowrate Q_{S0} and head H_{U0}), the location of the transient source $(x = x_T)$ and its response $H(x_T, t)$ are knowns. One pressure sensor is

14

mounted upstream of the transient source (i.e., $x = x_M$, $x_M < x_T$) and its head response $H(x_M, t)$ which contains the incident wave information (peak time $t_{x_M,in}^P$ and amplitude $(h_{amp})_{x_M}$) and leak-induced reflection information (peak time $t_{x_M,ref}^T$ and amplitude $(h_{amp})'_{x_M}$) is recorded. According to the time-delay between $t_{x_M,in}^P$ and $t_{x_M,ref}^P$, the distance d between the sensor and the leak can be determined for a given wave speed a_{VE} as $d = a_{VE}\left(t_{x_M,ref}^P - t_{x_M,in}^P\right)/2$. Thereafter, extracting the incident wave and the reflected wave at the sensor according to the procedure illustrated in Section 3 allows for obtaining the observed reflection coefficient $C_{ref\_M}^{Obs}$.

More specifically, for a single-frequency input signal, C_{ref_M} is a single value as the signal only contains one frequency component, however, for the more complex input signals of limited bandwidth (such as the impulse, step, sigmoid, Gaussian shape, etc.), C_{ref_M} is a vector, i.e., $\{C_{ref_M}(w_i)\}$, in which each element corresponds to its harmonic component w_i. Referring to the analytical reflection coefficient C_{ref_M} (denoted as $C_{ref\_M}^{Ana}$) in Eq. (20), if the pipeline's viscoelastic parameters are calibrated by the preliminary transient tests, $C_{ref\_M}^{Ana}$ is a function of leak ratio α and leak distance d. Based on this point, a new leak detection algorithm is proposed as elaborated in the following and illustrated in Fig. 4.
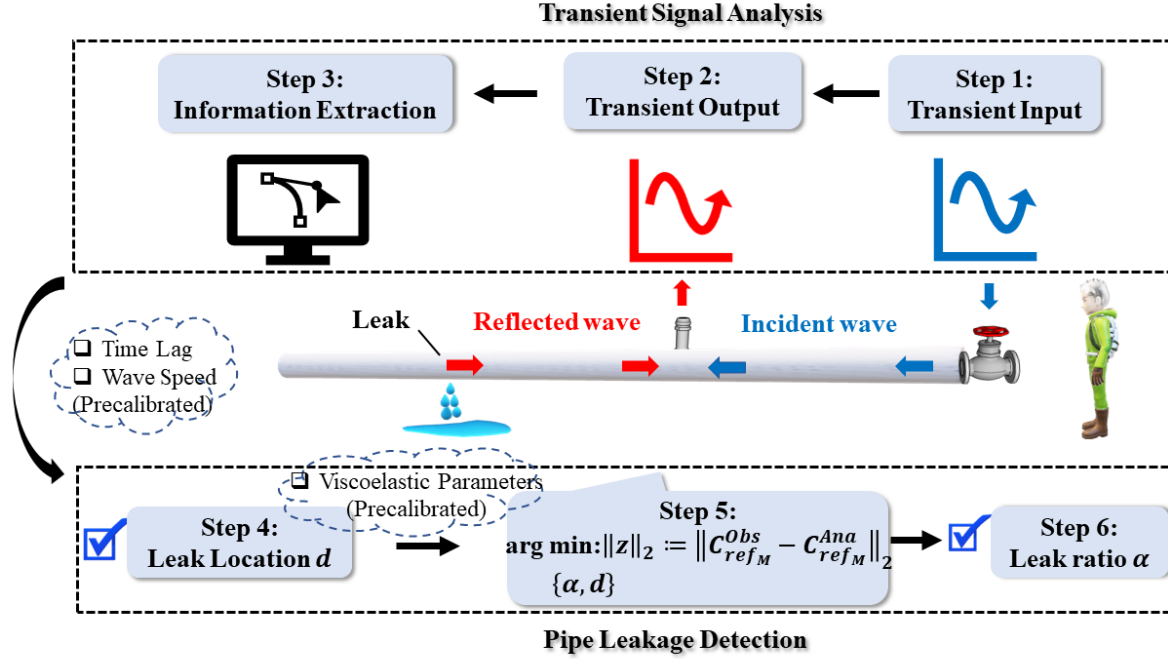
Figure 4 The overall flowchart of the developed TWRM for leak detection

The leak information α and d are the optimization arguments of the cost function $\|z\|_2$ which describes the difference between the vectors $C^{Ana}_{ref\_M}$ and $C^{Obs}_{ref\_M}$. By making the least-squares minimization $\|z\|_2 = \left\|C^{Obs}_{ref\_M} - C^{Ana}_{ref\_M}\right\|_2$, one can find the desired leak parameters (α, d). As mentioned in Section 2.1.2, since different leak scenarios can generate the same reflection coefficient, the optimization problem offers a group of optimum pairs $\{(\alpha, d)\}$ that satisfy $\arg\min\limits_{\{(a,d)\}}\|z\|_2$. Therefore, the estimated leak ratio α should be the one that corresponds to the detected d in the previous step, that means:

$$\{\alpha\} = \arg \quad \min: \left\|C^{Ana}_{ref\_M}(d) - C^{Obs}_{ref\_M}\right\|_2 \tag{25}$$

3. Results Validation and Analysis

3.1 Numerical validation by MOC results

To validate the analytical solution derived in Eq. (20), two different scales of numerical experiments in unbounded pipelines with one leak are applied for the illustration of the effects of unsteady friction and pipe wall viscoelasticity on the amplitude and phase shift of the transient waves. The pressure head $H_{U0} = 40$ m at pipe upstream is kept constant to simulate non-reflective upstream boundary and the upstream flow rate $Q_{S0} = 0.015$ m^3/s. For the testing viscoelastic pipeline, the quasi-steady friction factor $f_D = 0.015$ and the elastic wave speed is set as $a_0 = 400$ m/s. The finite difference scheme of the weighting convolution function and local acceleration terms in Eq. (2) follows the study by Zielke [54], and the MOC-based numerical scheme for the viscoelastic term follows that of Covas, et al. [17]. The corresponding system parameters for the four numerical experiments are listed in Table 1. To inspect the influence of input signals, transients are generated by two different perturbation operations at the downstream valve (DV): (i) single-frequency sinusoidal oscillation for numerical test Case 1A and 2A, and (ii) sigmoid-shaped impulse oscillation for numerical test Case 1B and 2B. After the perturbation duration T_V, the DV opening returns to its original state.

Table 1 System information for numerical tests

System No.	Case No.	L (m)	D (m)	e (m)	J_1 (Pa^{-1})	τ_1 (s)	y_L^*	α	y_M^*	Input Signal	I	γ_{fitted}
#1	1A	4000	0.2	0.01	1.0×10^{-11}	0.1	0.6	0.3	0.3	sinusoidal	0.3581	0.0322
	1B									sigmoid		
#2	2A	160	0.2	0.01	1.0×10^{-11}	0.01	0.6	0.3	0.3	sinusoidal	0.0143	0.1680
	2B									sigmoid		

For the assessment of unsteady friction, Duan, et al. [55] proposed a lumped dimensionless

system parameter $I = f_D ML/D$ to evaluate the relative importance of unsteady friction damping

to the total friction damping (quasi-steady friction and unsteady friction) during transients, where

$M = V/a_0$ is the Mach number. From that study [55], the following expression is adopted:

$$\gamma_{\text{fitted}} = 1.8 \times 10^{-1} e^{-4.85 I} \quad \text{for} \quad 10^{-2} \leq I \leq 1.0 \tag{26}$$

The larger the value of γ_{fitted}, the more important unsteady friction-induced damping to the total

friction damping. Consequently, it is evident that $\gamma_{\text{fitted}} = 3.22\%$ for system #1 and $\gamma_{\text{fitted}} =$

16.80% for system #2. This result indicates that the contribution of unsteady friction to the total

friction damping for system #1 is less than 5%, so its ignorance in modeling is acceptable. In

contrast, for system #2 it is higher than 10%, implying that the unsteady friction should be

considered in the simulation.

The 1D transient model is numerically solved by the method of characteristics (MOC) [6],

with the spatial steps set as 0.4 m for system #1 and 0.04 m for system #2. Meanwhile, to satisfy

the Courant condition for wave speed $a_0 = 400$ m/s, the computational time steps are set as

0.001 s for system #1 and 0.0001 s for system #2, respectively. The measurement collection of

the transient responses is executed at $y_M^* = 0.3$ locating between the leak and the DV.

3.1.1 Numerical verification results for sinusoidal perturbation

For a preliminary test, the transient source (pressure head) oscillates at DV with a single angular

frequency w_{in} for a time duration T_v, and then the DV returns to the initial state. Mathematically,

the injected pressure time signal can be expressed as:

$$H = \begin{cases} H_0 + H_0 \sin(w_{in} t); & t < T_v \\ H_0; & t \geq T_v \end{cases} \tag{27}$$

Based on the numerical results of transient simulation in the pipeline in Fig. 5, $\tilde{C}_{ref\_M}$ is calculated

by diving $(h_{amp})'_M$ by $(h_{amp})_M$ and the dimensionless phase difference θ^* at $y^*_{DV} = 0$ and $y^*_M = 0.3$ is calculated by Eq. (22).
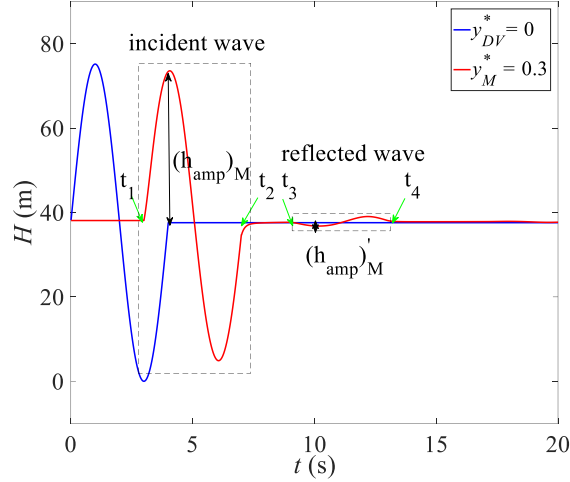
Figure 5 Pressure trace at the measurement location versus time for Case 1A ($w^* = 1.5$)

For evaluation, the relative difference between the numerical value $\tilde{Y}$ and analytical value Y (Y can be C_{ref_M} or θ^*), is used and represented by:

$$\varepsilon \; (\%) = \left| \frac{Y - \tilde{Y}}{Y} \right| \times 100 \tag{28}$$

The results of the relative difference ε for the two test systems under conditions of frictionless (FL), quasi-steady friction (SF), and total friction (SF+UF) are listed in Table 2 and Table 3. As expected, both SF and UF effects damp the wave amplitudes as indicated by the decrease of $\tilde{C}_{ref\_M}$ with these friction terms. The relatively small value of ε for the FL case which stems from a second-order approximation [17] of the retarded strain in the viscoelastic model for the MOC-based numerical simulation, validates the accuracy of this derived analytical results. It is also worth noting that the linearization of the quasi steady-friction term [56] and grid separation error [57] of the weighting function-based UF model in the MOC-based scheme may have a substantial

19

contribution to the ε value. Besides, UF-induced θ^* is more obvious than that by SF, which confirms the former results in the literature that the SF has little impact on phase shift while the UF does (although relatively small) [4].

Table 2 Numerical validation of derived leak-induced reflection coefficient ($w^* = 1.5$)

Case No.		FL		SF		SF+UF	
		MOC	ε (%)	MOC	ε (%)	MOC	ε (%)
1A	$(h_{amp})_M$ (m)	39.55	/	36.14	/	35.48	/
	$(h_{amp})'_M$ (m)	1.13	/	0.97	/	0.89	/
	$\tilde{C}_{ref\_M}$ (%)	2.85	4.9	2.68	8.2	2.52	11.0
2A	$(h_{amp})_M$ (m)	39.01	/	38.91	/	38.73	/
	$(h_{amp})'_M$ (m)	1.09	/	1.09	/	1.07	/
	$\tilde{C}_{ref\_M}$ (%)	2.80	4.5	2.79	4.7	2.76	5.1

**Table 3** Numerical validation of derived phase difference ($w^* = 1.5$)

Case No.		FL		SF		SF+UF	
		MOC	ε (%)	MOC	ε (%)	MOC	ε (%)
1A	θ^*	0.0115	2.3	0.0118	4.4	0.0158	1.7
2A	θ^*	0.0100	6.7	0.0100	6.7	0.0106	8.3

For Case 1A and 2A, a series of the single frequencies of sinusoidal wave oscillations at DV have been tested by following the procedure described in [36] to obtain the C_{ref_M} corresponding to the given incident frequency. The goodness of fit R^2 defined based on Pearson's chi-square parameter, is adopted to describe the accuracy of the developed analytical solution as follows:

$$R^2 = 1 - \sum_{i=1}^{N} \frac{\left(Y_i - \tilde{Y}_i\right)^2}{Y_i} \tag{29}$$

Fig. 6 shows the MOC-based numerical and analytical reflection coefficients match well for

a wide range of testing incident frequency $w^* \in (1.5, 300)$, since R^2 in all tested cases approach to 1.0. It is also observed that C_{ref_M} decreases with input wave frequencies for the three test conditions (FL, SF, SF+UF), which can be explained through the analytical damping operator $\mu_{VE,j}$, that is, the three frequency-dependent terms in the right-hand side of Eq. (7) for representing the effects of viscoelasticity, unsteady, and quasi-steady friction, respectively. Particularly, the induced damping effect of transient pressure waves is more evident for high-frequency components compared with that for low-frequency components [58, 59]. Although this kind of single-frequency oscillation of the input transient source is not common in real field tests [60], it contributes to the interpretation of the analytical solution as well as the understanding of the effective mechanisms. Physically, Duan, et al. [61] have explained this phenomenon from the energy dissipation perspective by the dissipation rate of these factors with frequency. The importance of the UF to the reflection coefficient in viscoelastic pipes is significant for high-frequency waves as we can see the discrepancy between FL/SF case and SF+UF case becomes large compared with that in the low-frequency range. In other words, using SF only is not enough to predict transient wave energy dissipation with sufficient accuracy in high-frequency disturbances [54].

21
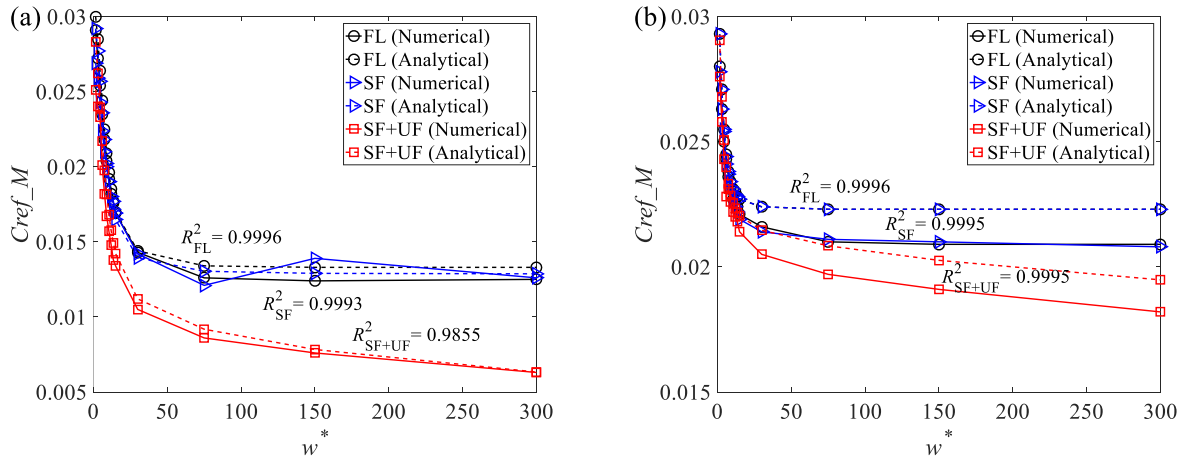
Figure 6 Results of leak-induced reflection coefficient for: (a) Case 1A; (b) Case 2A

### *3.1.2 Numerical verification results for sigmoid-shaped impulse*

For examining the influence of more complex incident signals, the flow oscillation imposed on the DV is set to be a sigmoid-shaped pulse which can be represented by the flow rate variation in time at the many typical valves' transient manipulation duration [62] as follows (with parameters setting listed in Table 4):

$$
Q = \begin{cases} Q_0 \left(1 - \dfrac{1}{1 + \mathrm{e}^{(-c_1)*(t - c_2)}}\right); & t < T_v/2 \\[2mm] Q_0 \left(1 - \dfrac{1}{1 + \mathrm{e}^{(-c_1)*(T_v - t - c_2)}}\right); & t \geq T_v/2 \end{cases} \tag{30}
$$

Compared to a single-frequency input signal, this kind of impulse signal covers a wide range of frequency bandwidths, and thus it is more practical. The transient pressure responses at the DV ($y_{DV}^* = 0$) and the measurement point ($y_M^* = 0.3$) with total friction (SF+UF) are plotted in Fig. 7. It can be observed that the shape of the incident wave becomes smoother as it propagates upwards from DV due to the combined effects of UF and VE [63, 64]. For analysis, the incident wave spectrum within 90% of the full lobe bandwidth and the corresponding reflected wave spectrum at $y_M^* = 0.3$ are used to calculate the numerical $\tilde{C}_{ref\_M}$ as performed in Zhang, et al. [36]. The results of the leak-induced reflection coefficient (C_{ref_M}) and the fitting goodness (R^2) are plotted in Fig. 8, exhibiting high accuracy of the analytical results in the whole tested bandwidth domain, particularly at high-frequency components for these two pipe systems.

Table 4 Sigmoid-shaped impulse oscillations parameters

Case No.	c_1	c_2	Tv(s)
1B	1500	0.005	0.02
2B	1500	0.005	0.1
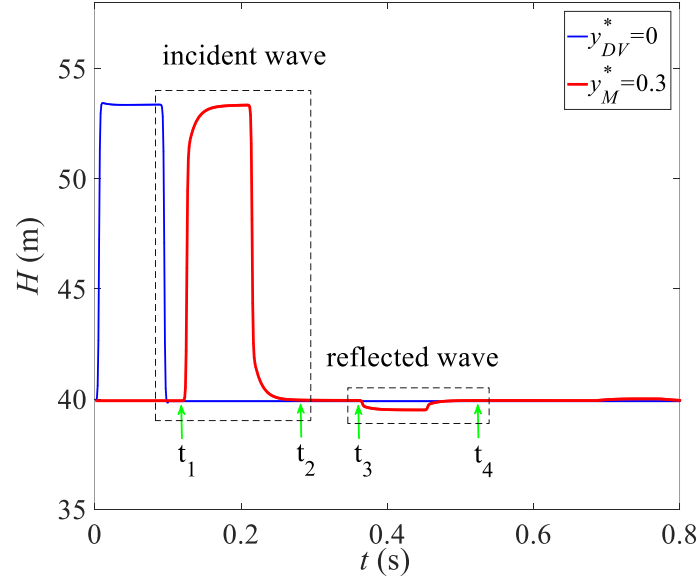
Figure 7 Pressure traces at the DV and measurement locations in the time domain for Case 2B

Figure 8 Results of leak-induced reflection coefficient for: (a) Case 1B; (b) Case 2B

3.2 Verification by laboratory experiment

The experimental test of the viscoelastic pipeline system at a constant water temperature and ambient temperature with negligible changes in Pan, et al. [25] is used to further validate and verify the derived analytical solution in this study for the leak-induced reflection coefficient. Since the temperature not only influences the density and viscosity of the fluid but also strongly changes the creep characteristics of the viscoelastic pipe, as a result, this impact is taken into consideration in the developed theoretical wave speed a_{VE} of the viscoelastic pipe, as seen in Eq. (6). A few

23

researchers, such as Gally, et al. [16] and Covas, et al. [5] have elaborately investigated in great detail the effect of temperature on the creep characteristics of the viscoelastic pipe-wall and on the transient behaviour in the water supply pipe via creep tests (under constant loads) and transient tests, respectively. They found that, with the increase of the temperature, (i) the pipe gets more flexible (i.e., larger values of the creep function); (ii) the wave period gets longer because of a slower a_{VE}; and (iii) larger damping of the peaks of the transient pressure wave. Nevertheless, all these impacts are automatically taken into consideration in the developed transient model. In other words, temperature affects the VE coefficients which themselves impact the transient behavior. This is the reason why in deriving the VE coefficients, the best approach is to calibrate them based on the measured transient responses. Since the key objective of the current study is not the calibration of the creep parameters of the pipe wall though being crucial for leak detection procedures [2, 25], we implicitly assumed the impacts of the temperature are included in the VE parameters.

In this testing system, the pipe material is HDPE with length $L = 166.28$ m, inner diameter $D = 0.0933$ m, thickness $e = 0.081$ m, dimensionless pipe axis constraint factor $\varphi = 1.23$ and elastic component of wave speed $a_0 = 377.15$ m/s. Specifically, this estimated wave speed a_0 is determined by the method of wavelet transform [11, 65] for better identification of characteristic times of the wavefront based on the preliminary laboratory transient tests. The system is bounded by a constant level $H_{U0} = 19.27$ m reservoir at upstream with the initial flow rate $Q_{S0} = 4.75$ m^3/s and a fully open DV. The leak is simulated by an orifice with a lumped discharge coefficient $C_d A_L = 6.8 \times 10^{-5}$ m^2, which locates at $y_L^* = 0.6334$ from the DV. Transient is generated by a sudden closure within $T_v = 0.119$ s of the DV. Detailed test configurations are summarized in Table 5. The pressure signal H_{exp} as shown in Fig. 9(a) at the DV is recorded by a

piezoresistive transducer with a sampling frequency $f_s = 1024$ Hz.

A single-side sigmoid-shaped curve (see Eq. (31) below) has been developed by Pan, et al. [25] to simulate the measured transient response within the valve closure duration as the boundary condition in the equivalent numerical RPV system (three-element K-V model). A developed multistage analysis procedure has been applied to calibrate the viscoelastic parameters of the pipeline by considering the total friction effect (SF+UF) [14].

$$H = 17.73 + \frac{25.59}{1 + 10^{41.28(0.0701-t)}} \tag{31}$$

Table 5 Experimental test system settings ([25])

L (m)	D (m)	e (m)	a (m/s)	Q_{S0} (m³/s)	H_{U0} (m)	φ	f_D	y_L^*	$C_d A_L$ (m²)	y_M^*	T_v (s)
166.28	0.0933	0.0081	377.15	4.75E-3	19.27	1.23	0.0193	0.6334	6.8E-5	1.0	0.119

In this study, only the first two-period dataset of the measured pressure trace rather than the whole trace is adopted due to the following reasons: (i) only the first reflection signal is used to calculate reflection coefficient; (ii) relatively important UF to transient amplitude damping during initial transient stage [4, 43]. With this dataset and analysis procedure, the calibration precision [28] defined in Eq. (32) is obtained as 0.6980 and the calibration result is shown in Table 6.

$$\sigma = \frac{\left(H_{exp} - H_{fitted}\right)^2}{N} \tag{32}$$

where H_{exp} is the experimental pressure head, H_{fitted} is the pressure head generated by the MOC model, and $N = 3500$ is the sampling number. Physically, these viscoelastic parameters are independent of initial flow conditions and boundary conditions [4], instead, they are intrinsic properties of the viscoelastic pipe-wall materials [4].

**Table 6** The calibrated viscoelastic parameters with a three-element K-V model.

J_1 (Pa^{-1})	τ_1 (s)	J_2 (Pa^{-1})	τ_2 (s)	J_3 (Pa^{-1})	τ_3 (s)
6.62E-11	0.2336	4.56E-11	0.0163	4.70E-10	10

As performed in [66], a correction process is carried out on the $\Delta H = H_{fiited} - H_{fiited,0}$ to convert the step signal (red solid line in Fig. 9(b)) into an impulse signal (blue solid line in Fig. 9(b)) in which the delayed time span (or time lag) equals to $50\ t_s$ (i.e., $\approx 0.1\ L/a$) to make sure that the incident wave marked by rectangle and the reflected wave marked by eclipse have a wide and smooth frequency spectrum [25]. Based on the explained signal extraction procedure in [36], the incident wave and reflected wave in Fig. 9(b) are transformed into the frequency domain by the Fast Fourier Transform to obtain experimental C_{ref_M} within 90% frequency bandwidth (i.e., $w = 0\sim30\ w_{th}$), which is then compared with the analytical results. The comparative results of reflection coefficient shown in Fig. 10 demonstrates very good agreement (i.e., $R^2 = 0.9608$) of the developed analytical formula. This experiment result implies that although the derived leak-induced reflection formula is based on the unbounded system, it still works for the bounded system. The slight discrepancy between experimental and analytical results are mainly attributed to: (i) difficulty in obtaining sufficiently accurate constitutive laws/continuity equation of viscoelastic pipe [1, 16]; (ii) additional unknown non-leak reflection and vibration signals captured by the sensor [67] that would directly influence the system's transient response; (iii) "frozen viscosity" assumption in weighting function approach for representing the UF effect which may deviate the real physical behaviour [57].
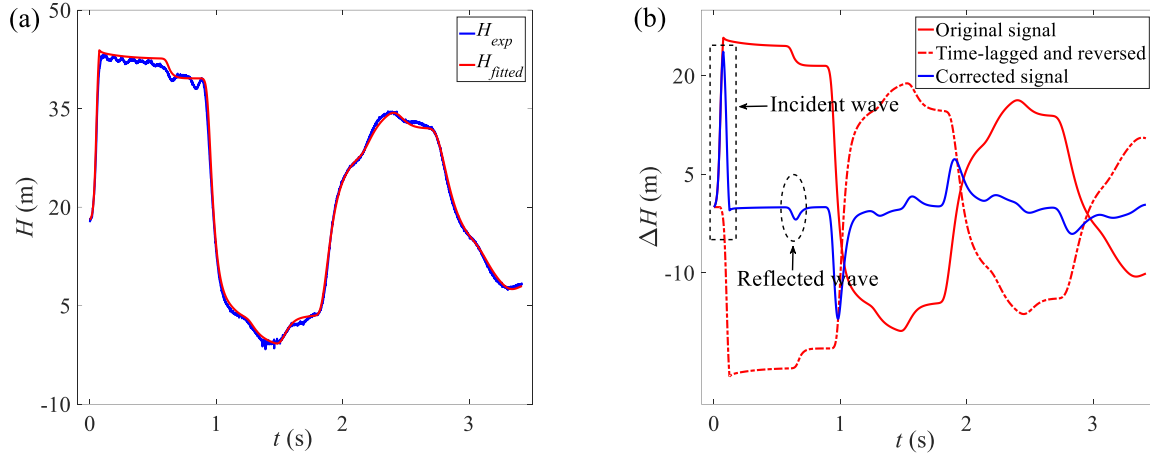
Figure 9 (a) Experimental measurement (with data from Pan, et al. [25]) and the numerical results of pressure trace; (b) Corrected pressure trace by the time-lag method.

In addition, the analytical reflection coefficient at the leak C_{ref_L} and at the measurement location C_{ref_M} from an equivalent scale elastic pipeline with the same leak are also plotted in Fig. 10 for comparative analysis. The difference between these two series gradually increases with frequency means that the unsteady friction term damps the wave more evidently for a high-frequency wave. This result manifests that, when using a high-frequency wave as the probing wave to detect the leak, one should take into account the influence of measurement distance. The large discrepancy occurs in C_{ref_M} of the elastic pipe (black line marked by triangle) and C_{ref_M} of the viscoelastic pipe (blue line marked by square) illustrates that the viscoelastic term could cause profound amplitude attenuation of transient waves, especially for high-frequency waves.
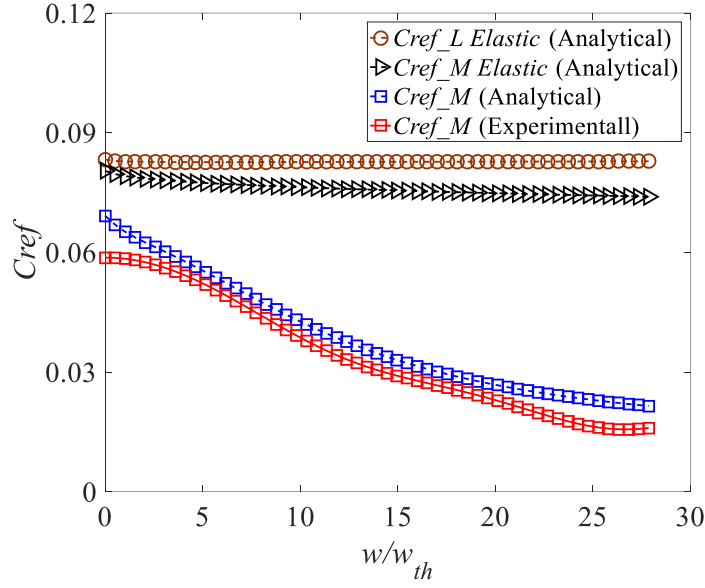
Figure 10 Comparison of the analytical and experimental leak-induced reflection coefficients.

3.3 Further analysis on the leak-induced reflection coefficient

With the validation of analytical results, a systemic qualification is further investigated and discussed on the different parameters affecting the derived reflection coefficient.

3.3.1 Influence of signal measurement distance

A long pipeline (system #1 listed in Table 1) with a leak ($y_L^* = 0.9, \alpha = 0.15$) is applied for testing the influence of different measurement locations ($y_M^* = 0.1 \sim 0.8$). The dimensionless distance between the leak and the measurement location is represented by $d^* = y_L^* - y_M^*$. Compared with the high-frequency waves, the damping of the low-frequency waves in the fluid is slighter, as indicated in Fig. 6 and Fig. 10, and the target pipes for the leakage identification in practical are usually long (several kilometers), therefore, in this study, we use low-frequency waves as the probing waves for the leak detection. For a given low-frequency input signal ($w^* =$

28

3) at DV (i.e., $y_{DV}^* = 0$), C_{ref_M} for three scenarios (i.e., FL, SF, and SF+UF respectively) are tested and the results are shown in Fig. 11. It can be concluded that, (i) for the FL case, C_{ref_M} located further from the leak (d^* is larger) is smaller than that closer to the leak (d^* is smaller), indicating that significant energy dissipation is caused by the viscoelastic effect (because of no friction effect); (ii) the phase difference between the incident and measured wave increases with the traveling distance; (iii) for the same measurement location, SF dampens the C_{ref_M} but has less influence on the phase difference, while UF could influence both C_{ref_M} and phase difference.
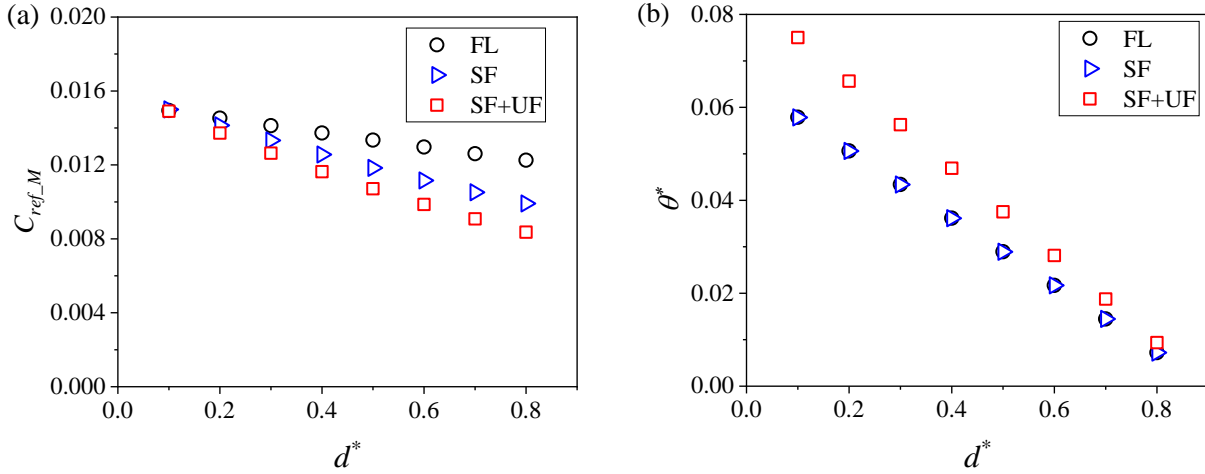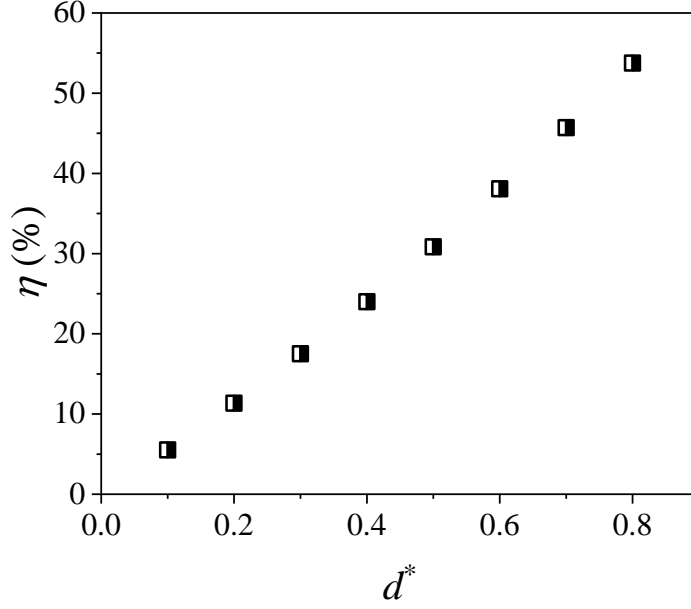

Figure 11 Influence of measurement distance to the reflection coefficient and phase difference

As mentioned in Section 1 and Section 2, C_{ref_M} as shown in Eq. (20) in the viscoelastic pipe is a function of the leak size, steady friction (SF), unsteady friction (UF), viscoelasticity (VE) of the pipe-wall material, and leak location (which is reflected at the distance d between the leak point and measurement point). Since many previous studies simplified the measured reflection coefficient as the reflection coefficient at the leak C_{ref_L} to inversely detect the leak, as a result, they ignored the interaction between d and the propagation operator $\mu_{VE,j}$ (which considers the SF,

UF, and VE effects together). But in this study, the impacts of these components are included and investigated, which is a manifestation of the transfer function essentially [11]. To further clarify the significance of these impacts, herein we show a detailed comparison in the following. Let η denote the simplification error as follows:

$$\eta(\%) = \left| \frac{C_{ref\_M} - C_{ref\_L}}{C_{ref\_M}} \right| \times 100 \tag{33}$$

Considering the numerical pipeline system #1 listed in Table l, we assume that one leakage ($y_L^* = 0.9$, $\alpha = 0.3$) for a varied measurement location range ($y_M^* = 0.1 \sim 0.8$). As can be seen from Fig. 12, η almost linearly increases with the dimensionless measurement distance d^* ($d^* = y_L^* - y_M^*$), particularly it reaches as high as 50% for the case when $d^* = 0.8$. This result illustrates the need for the modification of the reflection coefficient which is the initiative of this study. The above analysis indicates that, the distance between the leak and the installed sensor affects the magnitude of what is measured that is the combination of the traveled and reflected wave. This property along with the signal-to-noise ratio of the incident and reflected wave should be taken into consideration in practice so as to predict the order of accuracy in the localization and size estimation. In other words, if expecting a high accuracy in localization and size estimation, the sensor should be mounted close to the potential leak.

Figure 12 Influence of measurement distance to simplication error of the reflection coefficient.

3.3.2 Influence of leak ratio

An approximately linear relationship between C_{ref_M} and leak ratio α in the viscoelastic pipe is observed as in Fig. 13, which is similar to the elastic pipe case [36]. Fig. 13(a) indicates that, in comparison with FL case, both SF and UF could result in wave attenuation. However, SF is irrelevant to wave phase difference while UF could cause additional phase difference (as shown in Fig. 13(b)). Moreover, the observed phase difference keeps unchanged within the tested leak ratio α range for all three scenarios, which agrees with the findings in the literature [2].
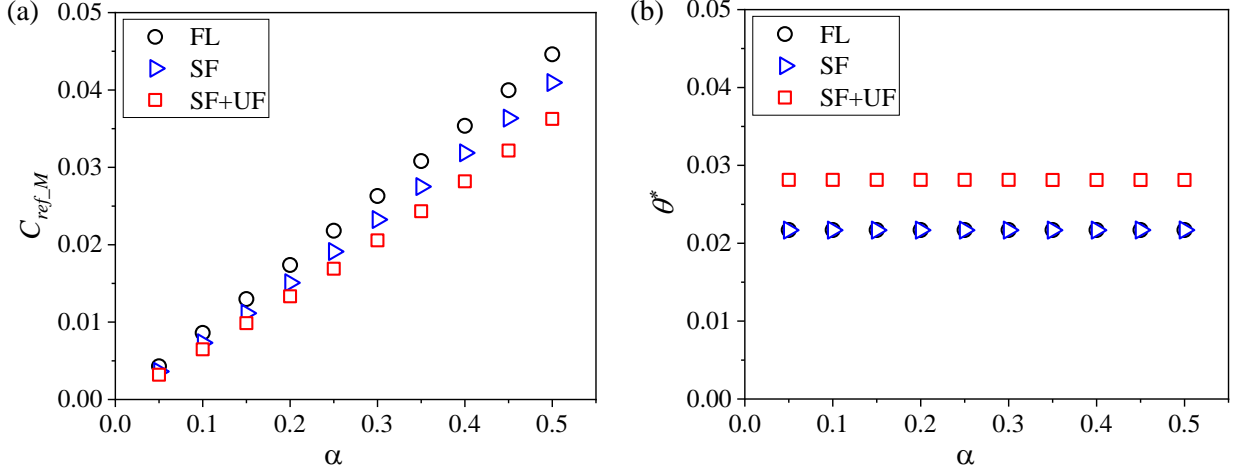
Figure 13 Influence of leak ratio to the reflection coefficient and phase difference

4. Implications to Leak Detection in Viscoelastic Pipelines

Numerical pipeline systems listed in Table 1 are applied to test the effectiveness of the developed method for leak detection. For the leak detection studies, it is assumed that the leak parameters (location and size) are unknowns, a sinusoidal wave excitation or sigmoid-shape curve perturbation on the DV is used as the transient source and the signal is measured at $x_M^* = 0.7$.

As mentioned, the wave speed is a time-dependent (or frequency-dependent) function that intrinsically relies on the creep parameters of the viscoelastic pipes, however, no firm wave speed formula in the time domain could be established if there are not plenty of preliminary measurements on the peak pressure's arrival times at several pipe locations or inverse calculations on the measured transient pressure to calibrate creep parameters. To facilitate the wave speed estimation for the leak location detection, the arrival time or traveling time of the wavefront at two transducers are employed to get the precalibrated average wave speed. With this simplification, the leak location d and the leak ratio α could be detected by optimization algorithms (as illustrated in Fig. 4) by most closely matching the measured reflection coefficient and the value modeled by the developed analytical formula, i.e., $\arg\min_{\{(\alpha,d)\}}\|\boldsymbol{z}\|_2$. The key parameters and detection results

32

are listed and marked in Table 7 and Figs.14~15, respectively.

Table 7 TRM-based leak detection results

System No.	Input Sigal	Case No.	Real Leak Information		Detected Results				Error	
			$(x_L^*)_{Real}$	$(\alpha)_{Real}$	$t_{M,in}^P$ (s)	$t_{M,ref}^T$ (s)	x_L^*	α	$\varepsilon_{x_L^*}$ (%)	ε_α (%)
#1	sinusoidal	1A	0.40	0.30	4.063	10.186	0.39	0.30	2.5	0.0
#2		2A	0.40	0.30	0.162	0.405	0.40	0.30	0.0	0.0
#1	sigmoid	S1	0.20	0.15	3.012	13.013	0.20	0.15	0.0	0.0
		S2	0.40	0.30	3.012	9.013	0.40	0.28	0.0	6.7
		S3	0.40	0.50	4.114	10.220	0.39	0.45	2.5	10.0
#2		S4	0.20	0.15	0.207	0.609	0.20	0.14	0.0	6.7
		S5	0.40	0.30	0.207	0.449	0.40	0.29	0.0	3.3
		S6	0.40	0.50	0.207	0.449	0.40	0.45	0.0	10.0

Figure 14 Leak detection results for the single frequency wave input:

for (a) Case 1A; (b) Case 2A

Figure 15 Leak detection results for the sigmoid curve input for system #1: (a) Case S1; (c) Case

S2; (e) Case S3; for system #2: (b) Case S4; (d) Case S5; (f) Case 6

In Figs.14~15, the cost function $\|z\|_2$ is visualized by colours. The colder the colour means the detected leak information (α, d) is closer to the real cases. Noting that the x-axis is transformed into the leak location from the upstream, i.e., $x_L^* = x_M^* - d$ for a more intuitive comparison. All these colormaps indicate $\min\|z\|_2$ occupy a slim blue band which corresponds to different

possible leak scenarios based on the measured $C_{ref\_M}^{Obs}$ which is also mentioned in [35, 68]. Hence, to detect the real leak size, the first step is to find the leak location based on the procedure in Section 2.2 and then to size the leak using the blue band.

For these two numerical pipeline systems of different scales, leak locations (i.e., x_L^*) are detected (i.e., $\varepsilon_{x_L^*} < 3\%$) for the tested cases herein and acceptable minor error (i.e., the $\varepsilon_\alpha < 7\%$) for the most common practical leak size (i.e., $\alpha < 0.3$). It is also noticed that even for the extra-large leak ratio scenarios (such as $\alpha = 0.5$), the detection errors are no more than 10%. Meanwhile, the detection results are also marked in Figs.14~15 in which the red cross indicates the real leak information and the purple circle indicates the detected leak result, respectively. All these detection cases indicate that the proposed analytical leak reflection coefficient could provide direct implications for leak size detection in viscoelastic pipelines.

It is also noted that other factors such as fluid-structure-interaction, surrounding noises, and complex boundaries (e.g., branches) are excluded in the results and analysis of this study [69], which requires further investigation in future works.

5. Summary and Conclusions

This paper investigates transient wave behaviour in a viscoelastic pipeline with leaks, to understand the wave-leak-viscoelasticity interactions and derive the accurate leak-induced wave reflection coefficient and phase difference in the time domain. Based on the one-dimensional transient flow model, considering quasi-steady friction (SF), unsteady friction (UF), measurement distance, and leak orifice formula, the analytical expression of transient wave reflection coefficient has been derived and applied for leak detection in this study. The obtained results are then validated and verified through different numerical and laboratory experiments, followed by the systematic

analysis of different system factors and flow conditions, including signal measurement distance and leak ratio for their impacts on the amplitudes and phases of the transient reflection waves. Finally, several numerical cases with different scales, different leak locations, and leak ratios under two types of transient oscillations have been conducted to evaluate the applicability of this developed analytical reflection formula to leak detection. The key results and findings are summarized as follows:

- signal measurement distance and leak ratio may greatly affect the magnitude changes of the transient reflection wave while the phase difference is relatively independent of leak ratio under reasonable conditions (e.g., leakage < 50%);

- Both friction effects (SF and UF) in the model may increase the errors of leak detection induced by the inaccuracy of viscoelastic parameters due to their nonlinear interactions during the transient wave propagation process along a viscoelastic pipeline;

- Results from previous studies are confirmed that both SF and UF can attenuate the wave, while UF causes phase difference but SF hardly does. Moreover, such frictional impacts on leak detection in a viscoelastic pipeline are highly dependent on the measurement points along the pipeline as well as the transient wave frequencies for the applications.

- The developed analytical leak reflection formula applies to the detection of a practical leak ratio (i.e., leakage < 50%) with an error less than 10% which illustrates the effectiveness and accuracy of this method.

Appendix - Analytical derivations

(A) Analytical solution of the transient wave equation in elastic pipes

To solve the equations in Eqs. (1) and (2), a Laplace transform [39] is taken for these equations and after some basic transformations under the relatively small perturbation conditions so that nonlinear term $\tilde{Q}^2$ can be neglected (e.g., $Q_0 \gg \tilde{Q}$),

$$\hat{\tilde{Q}}_x(x,s) + \frac{gA}{a_0^2}(s\hat{\tilde{H}}(x,s) - \tilde{H}(x,0)) = 0 \tag{A.1}$$

$$(\frac{1}{gA} + C_J\phi_w\sqrt{\frac{1}{s+\lambda}})s\hat{\tilde{Q}}(x,s) + \hat{\tilde{H}}_x(x,s) + \text{sign}(Q)\frac{f_D}{2gDA^2}2Q_0\hat{\tilde{Q}}(x,s) = 0 \tag{A.2}$$

where $\hat{\tilde{Q}}(x,s) = L\left(\tilde{Q}(x,t)\right) = \int_0^\infty e^{-st}\tilde{Q}(x,t)dt,\ s = jw = $ Laplace variable.

Taking the partial derivative of Eq. (A.1) with respect to x gives:

$$\hat{\tilde{Q}}_{xx}(x,s) + \frac{gA}{a_0^2}s\hat{\tilde{H}}_x(x,s) = 0 \tag{A.3}$$

and substituting $\hat{\tilde{H}}_x(x,s)$ in Eq. (A.2) into Eq. (A.3), it has:

$$\hat{\tilde{Q}}_{xx}(x,s) + \mu_E^2\hat{\tilde{Q}}(x,s) = 0 \tag{A.4}$$

in which

$$\mu_E^2 = -\left(\frac{s^2}{a_0^2} + \frac{s^2gAC_J\phi_w}{a_0^2}\sqrt{\frac{1}{s+\lambda}} + \text{sign}(Q)\frac{sgAR}{a_0^2}\right) \tag{A.5}$$

(B) Reflected wave at the leak point

The pressure and flowrate change at point B in Fig. 2 are:

$$H_B - H_{B0} = F_2 \tag{B.1}$$

$$Q_B - Q_{B0} = \frac{1}{k_{VE}} F_2 \qquad (B.2)$$

The mass conservation in the case of uniform pipe diameter at either side of the leak allows for

$$Q_A - Q_B = Q_L \Rightarrow V_A - V_B = \frac{Q_L}{A} \qquad (B.3)$$

$$Q_{A0} - Q_{B0} = Q_{L0} \Rightarrow V_{A0} - V_{B0} = \frac{Q_{L0}}{A} \qquad (B.4)$$

where Q_L is the magnitude of the leak discharge through the orifice. Omitting the pressure head loss at the leak point gives

$$H_B = H_A = H_L \qquad (B.5)$$

$$H_{B0} = H_{A0} = H_{L0} \qquad (B.6)$$

The leak is simulated by a metallic orifice (i.e., a rigid leak), which means its effective area $C_d A_L$ is constant and does not depend on the internal flow states and surrounding conditions. The relationship between leak rate Q_L and H_L is modeled by the orifice (or Torricelli's) equation as follows

$$Q_L = C_d A_L \sqrt{2gH_L} \qquad (B.7)$$

$$Q_{L0} = C_d A_L \sqrt{2gH_{L0}} \qquad (B.8)$$

where H_L = pressure head at a leak, C_d = discharge coefficient, A_L = leak area.

By combining the Eqs. (B.1) ~ (B.8), the reflected wave f_1 at the leaky point is expressed as

$$f_1 = -\frac{k_{VE}}{2}(Q_L - Q_{L0}) = -\frac{k_{VE}}{2} C_d A_L \sqrt{2g}\left(\sqrt{H_{L0} + F_1} + f_1 - \sqrt{H_{L0}}\right) \qquad (B.9)$$

which can be rearranged to a quadratic function for the unknown f_1. The solution to Eq. (B.9) is

$$f_1 = \frac{1}{8} \frac{(k_{VE}\alpha Q_{S0})^2}{H_{L0}} + \frac{k_{VE}}{2}\alpha|Q_{S0}| - \frac{1}{2}\frac{k_{VE}}{2}\frac{\alpha|Q_{S0}|}{\sqrt{H_{L0}}} \sqrt{\left(\frac{k_{VE}}{2}\frac{\alpha Q_{S0}}{\sqrt{H_{L0}}}\right)^2 + 4\left(\frac{k_{VE}}{2}\alpha|Q_{S0}| + H_{L0} + F_1\right)} \qquad (B.10)$$

(C) Transient wave's damping and reflection

Assuming that transient is generated by the downstream valve ($x = 0$), its amplitude is

$$h_{amp} = \left| \widehat{\widehat{H}}^{tr} \right| \qquad (C.1)$$

and propagating toward the leak location, the amplitude of this incident wave at point A (downstream of the leak) is

$$\left(h_{amp} \right)_A = \left| \widehat{\widehat{H}}^{tr} \right| e^{\mu_{VE,j} y_L} \qquad (C.2)$$

where y_L indicates the distance from the transient source to the leak point. As a result, at the leak ($y = y_L$), the reflected wave amplitude is

$$\left(h_{amp} \right)'_A = \left(h_{amp} \right)_A C_{ref\_L} \qquad (C.3)$$

The reflection again attenuates as propagates from point A to the measurement point ($y = y_M$)

$$\left(h_{amp} \right)'_M = \left(h_{amp} \right)'_A e^{\mu_{VE,j} d} \qquad (C.4)$$

where d indicates the distance between the leak and the measurement point. Finally, the reflection coefficient at the measurement point is represented by:

$$C_{ref\_M} = \frac{\left(h_{amp} \right)'_M}{\left(h_{amp} \right)_M} = \frac{C_{ref\_L} \left| \widehat{\widehat{H}}^{tr} \right| e^{\mu_{VE,j} y_M} e^{\mu_{VE,j} d} e^{\mu_{VE,j} d}}{\left| \widehat{\widehat{H}}^{tr} \right| e^{\mu_{VE,j} y_M}} = C_{ref\_L} e^{\mu_{VE,j}(2d)} \qquad (C.5)$$

Nomenclature

Roman Letters

a_0 = elastic wave speed (m/s);

A = pipe cross-sectional area (m^2);

A_L = orifice area (m^2);

C_d = leak discharge coefficient;

C_{ref_L} = leak-induced reflection coefficient at the leaky point;

C_{ref_M} = leak-induced reflection coefficient at the measurement point;

D = pipe diameter (m);

d = distance between the leak and the measurement point (m);

e = pipe-wall thickness (m);

e = Napier number;

E_0 = bulk modulus of elasticity (Pa);

f_D = Darcy-Weisbach friction factor;

f_{in} = frequency of the input transient signal (1/s);

f_1 = reflected wave at the leaky point (m);

F_1 = incident wave at the leaky point (m);

F_2 = transmitted wave at the leaky point (m);

g = gravitational acceleration (m/s);

h_{amp} = pressure oscillation amplitude of the incident wave (m);

$(h_{amp})'$ = pressure oscillation amplitude of the reflected wave (m);

H_A, H_B = pressure head at point A (leak downstream) and point B (leak upstream) (m);

H_L = pressure head at the leaky point (m);

H_{U0} = steady-state pressure head at pipe section upstream end or reservoir/tank (m);

$I = f_D M L / D$ = lumped dimensionless system parameter;

j = imaginary number;

$J_0 = 1/E_0$ = related to instantaneous (or elastic) response of the pipe wall's strain (1/Pa);

J_i = creep compliance of the spring of the i-th Kelvin-Voigt element;

L = pipe length (m);

$M = V_0/a_0$ = Mach number;

N_{KV} = total number of the Kelvin-Voigt elements;

Q_{S0} = initial flow rate at pipe section upstream (m^3/s);

Q_L = leak discharge (m^3/s);

Re = Reynolds number;

$s = jw$ = Laplace variable;

t = emporal coordinate (s);

$T_e = 2d/a_0$ wave time scale between the measurement point and the leak point (s);

T_{in} = Period of the input transient signal (s);

T_v = perturbation duration of the input transient signal (s);

w = angular frequency (rad/s);

V = velocity (m/s);

$w_e = 1/T_e$ frequency corresponding to the length d (rad/s);

$w^* = w/w_e$ dimensionless frequency;

w_{in} = frequency of the input transient signal (rad/s);

$w_{th} = 1/F_{th}$ = fundamental angular frequency for a bounded (rad/s);

x = spatial coordinate along the pipeline (m);

x_L = the leak distance from the pipe section upstream (m);

x_M = the measurement distance from the pipe section upstream (m);

x_T = the transient source distance from the pipe section upstream (m);

y_L = the leak distance from the pipe section downstream (m);

y_M = the distance between the measurement point and the pipe section downstream (m);

0 = subscript for representing steady-state.

Greek symbols

$\alpha = Q_{L0}/Q_{S0}$ = leak ratio (or leak size);

ε = relative difference/error;

θ = phase difference (rad);

τ_i = retardation time of the i-th Kelvin-Voigt element (s);

μ = propagation operator;

μ_r, μ_j = real and imaginary part of complex-value propagation operator μ;

υ = kinematic viscosity (m^2/s);

φ = pipe constraint coefficient;

ρ = density (kg/m^3).

σ = calibration precision

Superscript symbols

* : dimensionless;

$\sim$: perturbation from the mean;

$\wedge$: Laplace transform.

List of abbreviations

Ana: analytical;

DV: downstream valve;

exp: experimental;

E: elastic;

FL: frictionless;

Obs: observed;

"Real" = real part;

SF: steady friction;

tr: transmission;

UF: unsteady friction;

VE: viscoelastic;

ref: reflection.

References

[1] B. Pan, C. Capponi, S. Meniconi, B. Brunone, H.F. Duan, Efficient leak detection in single and branched polymeric pipeline systems by transient wave analysis, Mechanical Systems and Signal Processing, 162 (2022) 108084.

[2] X. Wang, J.R. Lin, M.S. Ghidaoui, S. Meniconi, B. Brunone, Estimating viscoelasticity of pipes with unknown leaks, Mechanical Systems and Signal Processing, 143 (2020) 106821.

[3] H.K. Aliabadi, A. Ahmadi, A. Keramat, Frequency response of water hammer with fluid-structure interaction in a viscoelastic pipe, Mechanical Systems and Signal Processing, 144 (2020) 106848.

[4] H.F. Duan, M.S. Ghidaoui, P.J. Lee, Y.K. Tung, Unsteady friction and visco-elasticity in pipe fluid transients, Journal of Hydraulic Research, 48 (2010) 354-362.

[5] D. Covas, I. Stoianov, J.F. Mano, H. Ramos, N. Graham, C. Maksimovic, The dynamic effect of pipe-wall viscoelasticity in hydraulic transients. Part I - experimental analysis and creep characterization, Journal of Hydraulic Research, 42 (2004) 516-530.

[6] M.H. Chaudhry, Applied Hydraulic Transients, Third Edition, New York: Springer, 2014.

[7] B. Brunone, C. Capponi, S. Meniconi, Design criteria and performance analysis of a smart portable device for leak detection in water transmission mains, Measurement, 183 (2021) 109844.

[8] J.Z. Gong, G.M. Png, J.W. Arkwright, A.W. Papageorgiou, P.R. Cook, M.F. Lambert, A.R. Simpson, A.C. Zecchin, In-pipe fibre optic pressure sensor array for hydraulic transient measurement with application to leak detection, Measurement, 126 (2018) 309-317.

[9] T.C. Che, H.F. Duan, P.J. Lee, S. Meniconi, B. Pan, B. Brunone, Radial pressure wave behavior in transient laminar pipe flows under different flow perturbations, Journal of Fluids Engineering, 140 (2018) 101203.

[10] B. Brunone, Transient test-based technique for leak detection in outfall pipes, Journal of Water Resources Planning and Management-ASCE, 125 (1999) 302-306.

[11] S. Meniconi, B. Brunone, M. Ferrante, In-line pipe device checking by short-period analysis of transient tests, Journal of Hydraulic Engineering-ASCE, 137 (2011) 713-722.

[12] B. Pan, A. Keramat, Y.T. She, H.F. Duan, A Novel Leak Localization Method Using Forward and Backward Transient Characteristics, Measurement, 194 (2022) 111065.

[13] G. Pezzinga, B. Brunone, D. Cannizzaro, M. Ferrante, S. Meniconi, A. Berni, Two-dimensional features of viscoelastic models of pipe transients, Journal of Hydraulic Engineering, 140 (2014) 4014036.

[14] B. Pan, H.F. Duan, S. Meniconi, K. Urbanowicz, T.C. Che, B. Brunone, Multistage frequency-domain transient-based method for the analysis of viscoelastic parameters of plastic pipes, Journal of Hydraulic Engineering, 146 (2020) 04019068.

[15] J.Z. Gong, A.C. Zecchin, M.F. Lambert, A.R. Simpson, Determination of the creep function of viscoelastic pipelines using system resonant frequencies with hydraulic transient analysis, Journal of Hydraulic Engineering, 142 (2016) 04016023.

[16] M. Gally, M. Gu¨ney, E. Rieutord, An investigation of pressure transients in viscoelastic pipes, Journal of Fluids Engineering, 101 (1979) 495-499.

[17] D. Covas, I. Stoianov, J.F. Mano, H. Ramos, N. Graham, C. Maksimovic, The dynamic effect of pipe-wall viscoelasticity in hydraulic transients. Part II—Model development, calibration and verification, Journal of Hydraulic Research, 43 (2005) 56-70.

[18] H.F. Duan, P.J. Lee, M.S. Ghidaoui, Y.K. Tung, System response function-based leak detection in viscoelastic pipelines, Journal of Hydraulic Engineering, 138 (2012) 143-153.

[19] P.J. Lee, H.F. Duan, M.S. Ghidaoui, B. Karney, Frequency domain analysis of pipe fluid transient behaviour, Journal of Hydraulic Research, 51 (2013) 609-622.

[20] A. Keramat, A.S. Tijsseling, Q. Hou, A. Ahmadi, Fluid-structure interaction with pipe-wall viscoelasticity during water hammer, Journal of Fluids and Structures, 28 (2012) 434-455.

[21] A. Keramat, B. Karney, M.S. Ghidaoui, X. Wang, Transient-based leak detection in the frequency domain considering fluid-structure interaction and viscoelasticity, Mechanical Systems and Signal Processing, 153 (2021) 107500.

[22] Y. Zhu, H.F. Duan, F. Li, C.G. Wu, Y.X. Yuan, Z.F. Shi, Experimental and numerical study on transient air-water mixing flows in viscoelastic pipes, Journal of Hydraulic Research, 56 (2018) 877-887.

[23] S. Meniconi, B. Brunone, M. Ferrante, Water-hammer pressure waves interaction at cross-section changes in series in viscoelastic pipes, Journal of Fluids and Structures, 33 (2012) 44-58.

[24] S. Meniconi, B. Brunone, M. Ferrante, C. Massari, Energy dissipation and pressure decay during transients in viscoelastic pipes with an in-line valve, Journal of Fluids and Structures, 45 (2014) 235-249.

[25] B. Pan, H.F. Duan, S. Meniconi, B. Brunone, FRF-based transient wave analysis for the viscoelastic parameters identification and leak detection in water-filled plastic pipes, Mechanical Systems and Signal Processing, 146 (2021) 107056.

[26] X. Wang, J.R. Lin, A. Keramat, M.S. Ghidaoui, S. Meniconi, B. Brunone, Matched-field processing for leak localization in a viscoelastic pipe: An experimental study, Mechanical Systems and Signal Processing, 124 (2019) 459-478.

[27] R.A. Silva, C.M. Buiatti, S.L. Cruz, J.A. Pereira, Pressure wave behaviour and leak detection in pipelines, Computers & Chemical Engineering, 20 (1996) S491-S496.

[28] D. Covas, H. Ramos, Case studies of leak detection and location in water pipe systems by inverse transient analysis, Journal of Water Resources Planning and Management, 136 (2010) 248-257.

[29] B. Brunone, B. Karney, M. Mecarelli, M. Ferrante, Velocity profiles and unsteady pipe friction in transient flow, Journal of Water Resources Planning and Management-ASCE, 126 (2000) 236-244.

[30] L.S. Suo, E.B. Wylie, Complex wavespeed and hydraulic transients in viscoelastic pipes, Journal of Fluids Engineering, 112 (1990) 496-500.

[31] X. Wang, M.S. Ghidaoui, J.R. Lin, Identification of multiple leaks in pipeline III: Experimental results, Mechanical Systems and Signal Processing, 130 (2019) 395-408.

[32] X. Wang, G.A. Camino, T.C. Che, M.S. Ghidaoui, Factorized wave propagation model in tree-type pipe networks and its application to leak localization, Mechanical Systems and Signal Processing, 147 (2021) 107116.

[33] L. Jönsson, M. Larson, Leak detection through hydraulic transient analysis, Pipeline systems, Springer, 1992, pp. 273-286.

[34] D. Covas, H. Ramos, N. Graham, C. Maksimovic, Application of hydraulic transients for leak detection in water supply systems, Water Science and Technology: Water Supply, 4 (2004) 365-374.

[35] C. Capponi, S. Meniconi, P.J. Lee, B. Brunone, M. Cifrodelli, Time-domain analysis of laboratory experiments on the transient pressure damping in a leaky polymeric pipe, Water Resources Management, 34 (2020) 501-514.

[36] Y. Zhang, H.F. Duan, A. Keramat, T.C. Che, On the leak-induced transient wave reflection and dominance analysis in water pipelines, Mechanical Systems and Signal Processing, 167 (2022) 108512.

[37] H.F. Duan, T.C. Che, P.J. Lee, M.S. Ghidaoui, Influence of nonlinear turbulent friction on the system frequency response in transient pipe flow modelling and analysis, Journal of Hydraulic Research, 56 (2018) 451-463.

[38] A.E. Vardy, J.M.B. Brown, Transient, turbulent, smooth pipe friction, Journal of Hydraulic Research, 33 (1995) 435-456.

[39] F. Oberhettinger, L. Badii, Tables of Laplace transforms, Springer Science & Business Media, 2012.

[40] A. Keramat, M. Fathi-Moghadam, R. Zanganeh, M. Rahmanshahi, A.S. Tijsseling, E. Jabbari, Experimental investigation of transients-induced fluid–structure interaction in a pipeline with multiple-axial supports, Journal of Fluids and Structures, 93 (2020) 102848.

[41] B.A. Khudayarov, K.M. Komilova, F.Z. Turaev, Numerical study of the effect of viscoelastic properties of the material and bases on vibration fatigue of pipelines conveying pulsating fluid flow, Engineering Failure Analysis, 115 (2020) 104635.

[42] S. Mukherjee, G.H. Paulino, The elastic-viscoelastic correspondence principle for functionally graded materials, Journal of Applied Mechanics-Transactions of the ASME, 70 (2003) 359-363.

[43] G. Pezzinga, B. Brunone, S. Meniconi, Relevance of pipe period on Kelvin-Voigt viscoelastic parameters: 1D and 2D inverse transient analysis, Journal of Hydraulic Engineering, 142 (2016) 04016063.

[44] M. Louati, M.S. Ghidaoui, M.M. Tekitek, P.J. Lee, Wave-leak interaction in a simple pipe system, Journal of Hydraulic Engineering, 146 (2020) 04020013.

[45] E. Kreyszig, Advanced Engineering Mathematics, 10th Eddition, Wiley, 2009.

[46] E.B. Wylie, Fluid Transients in Systems, Englewood Cliffs, NJ: Prentice Hall, 1993.

[47] D. Maudsley, Errors in the simulation of pressure transients in a hydraulic system, Transactions of the Institute of Measurement and Control, 6 (1984) 7-12.

[48] C.P. Liou, Pipeline leak detection by impulse response extraction, Journal of Fluids Engineering, 120 (1998) 833-838.

[49] M. Ferrante, S. Meniconi, B. Brunone, Local and global leak laws, Water Resources Management, 28 (2014) 3761-3782.

[50] H. Moiler, Loudspeaker phase measurements, transient response and audible quality, Brüel & Kjær Application Notes, presented at the 48th Audio Engineering Society Convention California, 1974.

[51] K.Y. Lee, C.F. Huang, S.S. Huang, K.N. Huang, M.S. Young, A high-resolution ultrasonic distance measurement system using vernier caliper phase meter, IEEE Transactions on Instrumentation and Measurement, 61 (2012) 2924-2931.

[52] S.C. Chang, J.G. Lin, L.K. Chien, Y.F. Chiu, An experimental study on non-linear progressive wave-induced dynamic stresses in seabed, Ocean Engineering, 34 (2007) 2311-2329.

[53] H. Yadav, A. Venugopal, S.V. Prabhu, A. Agrawal, Study on connecting tube dynamics for transient pressure measurement, Sādhanā: Academy Proceedings in Engineering Sciences, 45 (2020) 1-12.

[54] W. Zielke, Frequency-dependent friction in transient pipe flow, Journal of Basic Engineering Transactions of the ASME, 90 (1968) 109-115.

[55] H.F. Duan, M.S. Ghidaoui, P.J. Lee, Y.K. Tung, Relevance of unsteady friction to pipe size and length in pipe fluid transients, Journal of Hydraulic Engineering, 138 (2012) 154-166.

[56] C. Capponi, A.C. Zecchin, M. Ferrante, J.Z. Gong, Numerical study on accuracy of frequency domain modelling of transients, Journal of Hydraulic Research, 55 (2017) 813-828.

[57] J. Vitkovsky, M. Stephens, M. Lambert, J. Vítkovský, M. Stephens, A. Bergant, A. Simpson, M. Lambert, Numerical error in weighting function-based unsteady friction models for pipe transients, Journal of Hydraulic Engineering, 132 (2006) 709-721.

[58] J.Z. Gong, M.F. Lambert, S.T.N. Nguyen, A.C. Zecchin, A.R. Simpson, Detecting thinner-walled pipe sections using a spark transient pressure wave generator, Journal of Hydraulic Engineering, 144 (2018) 06017027.

[59] J. Muggleton, M. Brennan, R. Pinnington, Wavenumber prediction of waves in buried pipes for water leak detection, Journal of Sound and Vibration, 249 (2002) 939-954.

[60] M.F. Ghazali, Leak detection using instantaneous frequency analysis, Ph.D. Thesis, University of Sheffield, UK, 2012.

[61] H.F. Duan, M.S. Ghidaoui, Y.K. Tung, Energy analysis of viscoelasticity effect in pipe fluid transients, Journal of Applied Mechanics, 77 (2010) 044503.

[62] M. Ferrante, Transients in a series of two polymeric pipes of different materials, Journal of Hydraulic Research, 59 (2021) 810-819.

[63] H. Ramos, D. Covas, A. Borga, D. Loureiro, Surge damping analysis in pipe systems: modelling and experiments, Journal of Hydraulic Research, 42 (2004) 413-425.

[64] A. Bergant, A.S. Tijsseling, J.P. Vítkovský, D.I. Covas, A.R. Simpson, M.F. Lambert, Parameters affecting water-hammer wave attenuation, shape and timing—Part 1: Mathematical tools, Journal of Hydraulic Research, 46 (2008) 373-381.

[65] M. Prek, Wavelet analysis of sound signal in fluid-filled viscoelastic pipes, Journal of Fluids and Structures, 19 (2004) 63-72.

[66] P.J. Lee, Using system response functions of liquid pipelines for leak and blockage detection, Ph.D. Thesis, the University of Adelaide, Adelaide, Australia, 2005.

[67] X. Wang, M.S. Ghidaoui, Pipeline leak detection using the matched-field processing method, Journal of Hydraulic Engineering, 144 (2018) 04018030.

[68] B. Brunone, S. Meniconi, C. Capponi, Numerical analysis of the transient pressure damping in a single polymeric pipe with a leak, Urban Water Journal, 15 (2018) 760-768.

[69] H.F. Duan, B. Pan, M.L. Wang, L. Chen, F.F. Zheng, Y. Zhang, State-of-the-art review on the transient flow modeling and utilization for urban water supply system (UWSS) management, Journal of Water Supply: Research and Technology-AQUA, 69 (2020) 858-893.